22nd IAHR International Symposium on Ice
Singapore, August 11 to 15, 2014

Crystal Orientation in Ice Frozen from Fresh and Brackish Water

Stephanie Grothe[1], Kenneth Hughes[1], Pat Langhorne[1]

[1]*Department of Physics, University of Otago, P.O. Box 56, Dunedin, New Zealand*
sgrothe@phas.ubc.ca
kenneth.hughes@otago.ac.nz
pat.langhorne@otago.ac.nz

Seven experiments on ice grown in water of differing salinities ($0 < S < 3.0$ ppt) are undertaken to determine the most important drivers of ice crystal orientation. In six experiments, the water is not stirred, the ice cover is unseeded, and ice grows at approximately 1.6 mm hr^{-1}. Under these conditions we find that crystal *c*-axis inclinations are predominantly vertical at water salinities less than 1.2 ppt and predominantly horizontal at salinities greater than 2.0 ppt. We also observe a transition from a planar to cellular interface between these salinities. Together, these observations suggest that the change in dominant crystal orientation is explained by constitutional supercooling and its influence on the morphological instability of the ice–water interface. However, in the ice that forms initially at the ice–air interface, the crystal orientation appears to be controlled by the temperature profile in the water close to the interface. The experimental evidence suggests that *c*-axis vertical orientations are more likely in the initial skim if there is a hydrodynamically stable layer at the interface.

Proceedings of the 22nd IAHR International Symposium on Ice
Copyright © 2014 IAHR 2014 Organizers. All rights reserved.
ISBN: 978-981-09-0750-1
doi:10.3850/978-981-09-0750-1_1253

1. Introduction

Crystal orientation in ice influences its strength and albedo (e.g. Knight, 1962; Gow and Ueda, 1989) and, in turn, the formation and decay of ice. Usually the crystal *c*-axis distribution is determined by geometric selection, the mechanism by which crystals in favoured orientations outgrow their neighbours. The favoured orientation is usually that for which heat and/or impurities can be transported most rapidly from the interface. In turn, this rate is determined by the interface morphology and the fluid dynamic conditions at the ice–water interface.

When impure water freezes, impurity is rejected at the solid–liquid interface. This impurity reduces the freezing point close to the freezing interface. The differing rates of diffusion of heat and impurity cause the liquid immediately adjacent to the interface to become constitutionally supercooled. Any perturbation on the interface therefore finds itself in supercooled water and grows rapidly. Constitutional supercooling is a necessary condition for the 2D cellular structure that is readily observed at the sea ice–water interface. However it is not sufficient and theories of interface morphological stability are needed to predict cellular spacing (Wettlaufer, 1992; Weeks, 2010).

This dependence on solute content means that the morphology of the ice–water interface and the orientation of the crystal *c*-axes differ for freshwater ice and sea ice. In freshwater, ice grows with a planar surface, and crystal orientations are controlled by environmental factors. A preferred orientation develops in which crystal *c*-axes are either predominantly vertical or predominantly horizontal. The former is expected during quiet (non-turbulent) freezing, whereas the latter is expected if the ice is seeded (Gow, 1986). Gow (1986) noted that his observations conflicted with some previous observations; however, a recent study by Müller-Stoffels et al. (2009) supports Gow's (1986) rule. These authors explain the rule by providing evidence for an earlier hypothesis that the temperature profile in the water during freezing controls the crystal orientation (e.g., Perey and Pounder, 1958) and noting that partial melting of ice seeds influences the temperature gradient.

In contrast to freshwater ice, crystal orientations in sea ice below 4–5 cm are independent of the ice above, and the movement of the underlying fluid has an influence. The addition of impurity to the interfacial liquid upon freezing increases this liquid's density, thereby causing a hydrodynamic instability at the interface and hence convective mixing. Because of this, crystals in columnar sea ice have a strong tendency to grow with their *c*-axis in the horizontal plane, i.e., perpendicular to the movement of the ice–water interface. This is the orientation in which salt can be most rapidly removed from the intercellular grooves by fluid transport. That is, the crystals grow with their basal plane (fast growth plane) directed downward into the thin layer of water that is constitutionally supercooled. The interface develops a millimetre-scale cellular morphology (Weeks and Ackley, 1986) of ice lamellae or platelets, with brine trapped between the platelets.

In previous work a transition from ice resembling freshwater ice to ice resembling sea ice has been estimated to occur at salinities of $0.6 < S < 3.0$ ppt (Palosou, 1961; Weeks and Lofgren, 1967). At these low salinities (below 24.7 ppt), the temperature of maximum density in the fluid is above the freezing point, so there will be a hydrodynamically stable layer at the surface in an unstirred fluid until freezing begins.

Table 1. Summary of six experiments. Median inclinations $\tilde{\theta}$ are reported with their respective upper and lower quartiles in brackets.

S_0	S_f	d	T_0	Δt	t_{ice}	v	G_S	$\tilde{\theta}$ (top)	$\tilde{\theta}$ (mid.)	$\tilde{\theta}$ (bot.)
ppt	ppt	cm	°C	min	hr	mm hr^{-1}	K m^{-1}	°	°	°
0.0	0.0	7.0	19.5	60	38	1.6 ± 0.1	60 ± 2	6 (6, 8)	8 (6, 11)	6 (5, 9)
0.4	0.5	7.5	8.0	15	41	1.7 ± 0.1	60 ± 3	8 (6, 61)	7 (6, 14)	9 (6, 11)
0.6	-	6.5	14.0	10	32	1.6 ± 0.1	66 ± 3	5 (5, 8)	2 (2, 4)	0 (0, 8)
1.2	1.4	8.0	3.3	5	42	1.6 ± 0.1	65 ± 3	-	11 (11, 11)	17 (15, 17)
2.0	2.2	6.2	14.7	2	28	1.6 ± 0.1	59 ± 4	72 (56, 80)	71 (60, 80)	80 (74, 90)
3.0	3.5	8.7	2.9	5	43	1.3 ± 0.1	73 ± 6	5 (5, 5)	23 (6, 61)	76 (66, 90)

Here we report on seven experiments on ice grown in a tank containing brackish water of various salinities ($0 < S < 3.0$ ppt). In these conditions we therefore expect a low density, hydrodynamically stable layer prior to freezing. The resulting crystal orientations and ice–water interface morphologies are observed. We explore mechanisms that would be expected to control crystal orientation: constitutional supercooling (Tiller et al., 1953; Weeks and Ackley, 1986; Gow et al., 1992), the stability of the interface to perturbations (Wettlaufer, 1992), and the role of transport of heat and salt at the interface (Weeks, 2010). Given the salinities employed here, we obtain results pertinent to ice growing in regions such as the Baltic Sea, the northern Caspian Sea, and Arctic fiords and lakes, all of which exhibit salinities that straddle the freshwater ice to sea ice transition (Palosuo, 1961; Dumont, 1998; Ryves et al., 2004; Granskog et al., 2006).

2. Methods

We formed ice in a 63×125 cm tank (width × length) filled with tap water to a height of 50 cm. We mixed in sodium chloride to achieve the desired salinities, and these were measured with a YSI 3100 conductivity meter at the beginning (S_0) and end (S_f) of each experiment. We obtained approximately one-dimensional heat flow by insulating the tank sides with polystyrene then cooling the surrounding room to −20°C. Table 1 summarises six of our experiments conducted at approximately the same ice growth velocity.

An array of 21 Betatherm 10K3A542I thermistors (see Figure 1a) recorded the temperature to ±0.03°C in the water, ice, and air above the ice surface at intervals of Δt (see Table 1). The thermistor records for the $S = 1.2$ ppt experiment are typical of all experiments and are shown in Figure 1b. Four dependent variables for each experiment are derived from these records (Table 1): T_0, initial water temperature before cooling began; t_{ice}, duration of ice growth after freezing began; v, growth velocity; and G_S, temperature gradient within the ice. Ice thickness versus time and ice temperature versus ice depth are both well represented by linear functions. Hence, both v and G_S are evaluated using a linear fit from 4–7 thermistors less than 7 cm below the air–ice interface. G_S was evaluated at the end of the experiment.

Samples ($7 \times 7 \times 1$ cm) were cut from the centre of the ice sheet after 6–9 cm of growth (final ice thickness is denoted d in Table 1). In each experiment, a horizontal thin section was prepared for the top, middle (3.0–3.9 cm), and bottom (6.1–7.7 cm) of the ice sheet. One vertical thin section through the ice cover was also taken. Thin sections were prepared by freezing thick sections onto a glass slide and thinning them to 0.4 mm thickness with a Leica microtome.

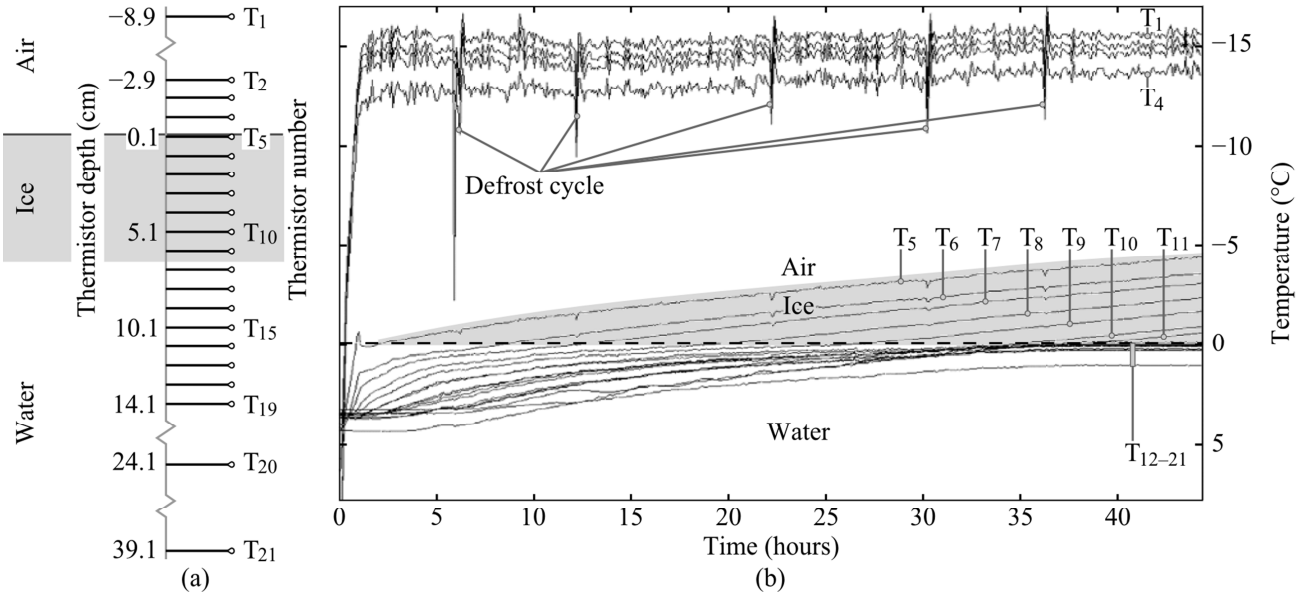

Figure 1. (a) Position of each thermistor. Thermistors $T_{2–19}$ are each separated by 1 cm. (b) A typical temperature record. Defrost cycles occur every 5–10 hours. Note the temperature axis is inverted to allow the thermistor records to correspond with (a).

Thin sections were placed on a universal stage to determine the inclination θ and azimuth ϕ of crystal *c*-axes (Langway, 1958). Inclinations of 0° and 90° correspond to vertical and horizontal *c*-axes, respectively. Each angular measurement has a ±5° uncertainty. To adequately sample each thin section, crystal orientations were measured at each intersection of a 1 × 1 cm grid. This meant 40–70 measurements were recorded for each section. Many crystals extended over several grid points meaning that their orientations were recorded multiple times. Therefore, *c*-axis distributions presented here represent areal coverage. For each thin section, we summarise the *c*-axis distributions by reporting median inclination $\tilde{\theta}$ and the associated lower and upper quartiles (see Table 1). Calculating means and standard deviations is inappropriate here because *c*-axis distributions do not follow a normal distribution and each inclination value is contained in the range 0–90°.

3. Influence of Salinity on Crystal Orientation and Ice–Water Interface Morphology

Crystals in the ice grown from freshwater exhibit predominantly vertical *c*-axes: at the top, middle, and bottom of the ice cover, the median inclinations $\tilde{\theta}$ are 6°, 8°, and 6°, respectively (Table 1, Figure 2). Hence, our freshwater ice observations are consistent with unseeded ice growth experiments by Gow (1986) and Müller-Stoffels et al. (2009).

At low salinities ($0 < S \leq 1.2$ ppt), *c*-axes are still predominantly vertical at all depths. There is an overall increase in the areal coverage of crystals with a horizontal or near-horizontal *c*-axis (Figure 2), but the trend is as large as the uncertainty. Visual inspection of the vertical thin sections for these experiments shows that *c*-axis horizontal crystals are wedged out by their vertical counterparts, typically within 2–4 cm of growth. However, we do not find a decreasing trend in $\tilde{\theta}$ with depth because a small number of new *c*-axis horizontal crystals appear deeper in the ice.

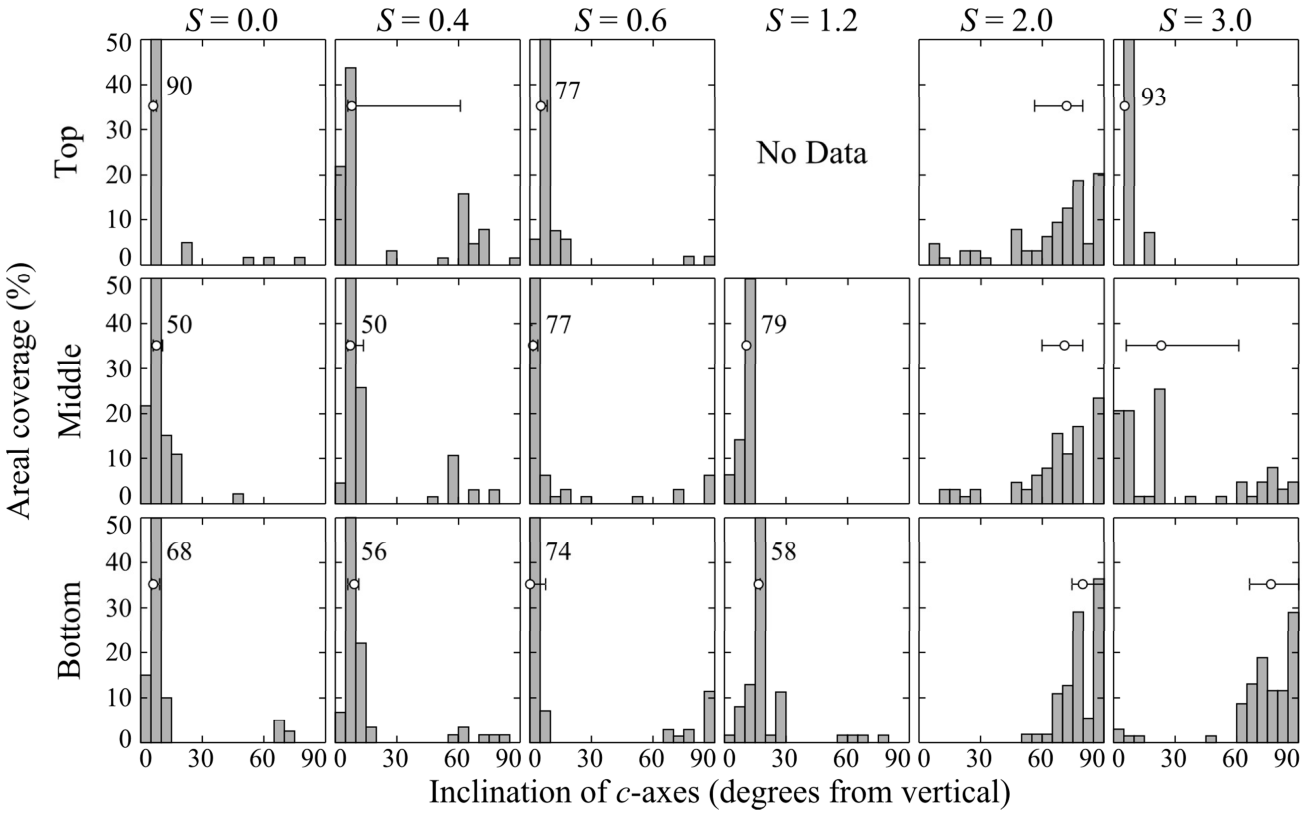

Figure 2. (a) Inclination angle distribution for different salinities and the three depths within each ice cover where thin sections were created. In each experiment, ice grew at $1.3 \leq v \leq 1.7$ mm hr^{-1}. Each bar represents a 5° bin. If a bar equals or exceeds 50%, its magnitude is noted beside. Circles with error bars represent the median inclination and associated lower and upper quartiles (see Table 1).

Increasing salinity to 2.0 ppt causes a transition in crystal orientation (Figure 2). Crystals with a horizontal *c*-axis now clearly dominate. The *c*-axis distributions at the middle and bottom of the ice cover now resemble those of columnar sea ice. Indeed, not a single crystal with an inclination of $< 5°$ is observed during this experiment. We note that the dominance of *c*-axis horizontal crystals is less pronounced in the $S = 3.0$ ppt experiment and attribute this to differing conditions during initial freezing (see Section 4). Overall, our observations (i) are consistent with Weeks and Lofgren (1967), who observed a transition between "lake ice" and "salt ice" between 1 ppt and 2 ppt in unstirred water, and (ii) suggest that a transition in the dominant growth mechanism occurs between 1.2 ppt and 2.0 ppt for a growth velocity of 1.6 mm hr^{-1}.

Thin section photographs reveal a visual characteristic exclusive to the $S \geq 2.0$ ppt experiments that gives further evidence for cellular growth. Sub-grain features appear in the form of thin lines parallel to the crystal boundaries. These were regularly spaced with a typical separation of 0.4 mm ($S = 2.0$ ppt) and 0.8 mm ($S = 3.0$ ppt). Such features are consistent with pockets of brine trapped between plates of pure ice (e.g., Weeks and Ackley, 1986). It therefore follows that the ice–water interface was cellular. Each of the three horizontal thin sections for the $S = 2.0$ ppt experiment are shown in Figure 3. It can be seen that the needle-like elongated crystals become broader with increasing depth and their boundaries roughen. This same behaviour was observed in the middle and bottom thin sections in the $S = 3.0$ ppt experiment.

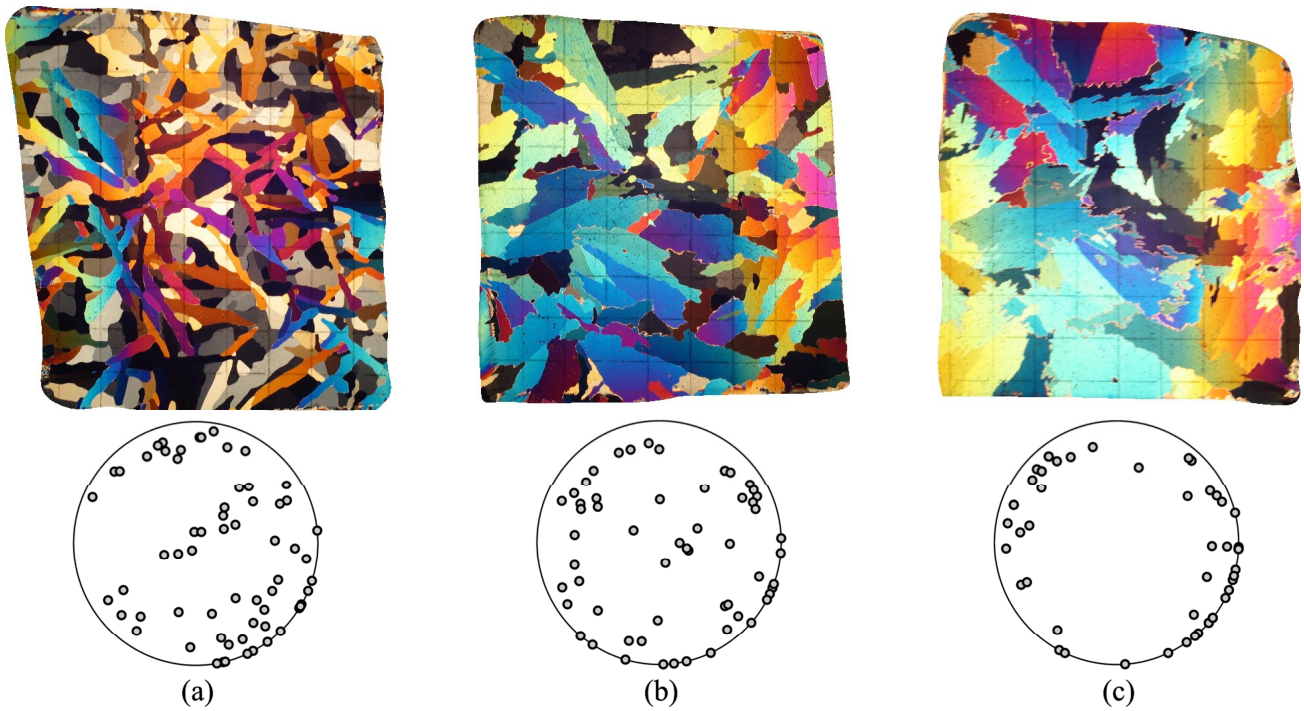

Figure 3. Horizontal thin sections and corresponding Schmidt net plots from the $S = 2.0$ ppt experiment. (a) Top, (b) middle, and (c) bottom. The grids visible in the background of the thin sections are 1×1 cm. Points on the edge of the circle correspond to horizontal *c*-axes. The top thin section originates from a different position in the ice cover to the lower two.

Our experiments were undertaken in controlled conditions, so it is likely that seeding of the air–water interface at the moment of initial freezing is negligible. We therefore examine the role of constitutional supercooling in determining the observed *c*-axis distributions. Constitutional supercooling is a necessary, but not sufficient, condition for the formation of cellular interface (Weeks, 2010). Constitutional supercooling occurs if (e.g., see derivation in Weeks, 2010) $S_0 v / G_s > A$, where A depends on the properties of the liquid, solid and impurity. We may regard the left hand side of the inequality as a measure of the tendency to form a non-planar interface. In Figure 4a we examine inclination angle as a function of $S_0 v / G_s$. There appears to be a strong dependence of crystal orientation on constitutional supercooling at the bottom depths (6.1–7.7 cm), with the observed planar–cellular transition coinciding with a change in *c*-axes from predominantly vertical to predominantly horizontal.

4. Crystal Orientation in the Initial Layer

The initial crystal orientation cannot be explained by constitutional supercooling because there is no clear relationship between *c*-axis inclination and salinity in Figure 2 for the top thin sections. Instead, we hypothesise that the proportion of *c*-axis vertical crystals will increase with the thickness of a stably stratified layer at the air–water interface. A quiescent zone will lead to a higher proportion of *c*-axis vertical crystals because such crystals have their fast-growth plane oriented parallel to the layer of coldest water, i.e., the layer immediately at the air–water interface.

Under the presumption that salinity of water in the tank is uniform prior to freezing, the temperature profile will determine the density profile. For the range of salinities employed in this

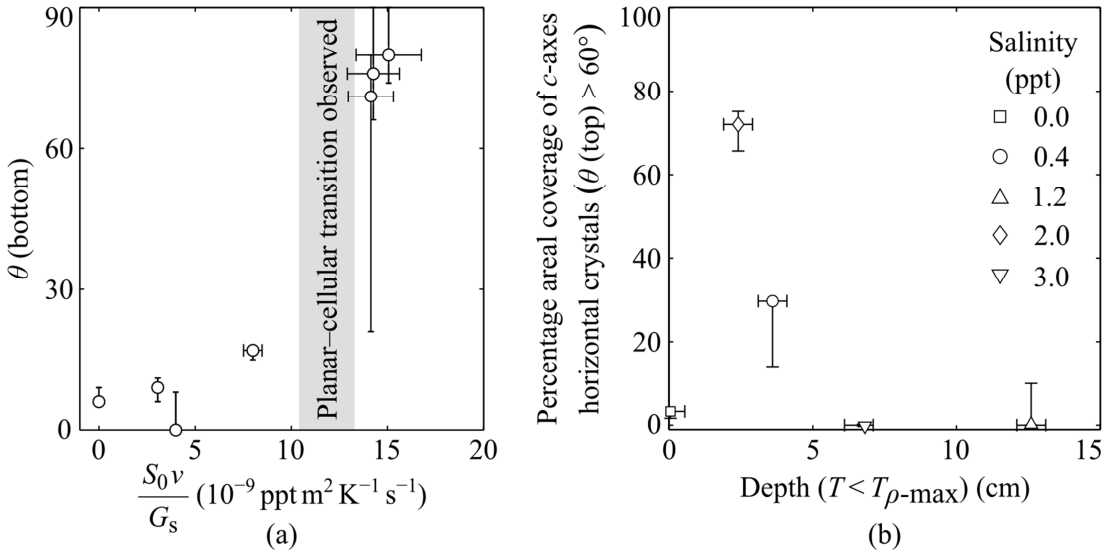

Figure 4. Factors explaining the observed crystal orientation in the bottom and top thin sections. (a) Inclination angle in the bottom thin sections (depth = 6.1–7.7 cm) as a function of $S_0 v / G_s$. The grey bar denotes the value of $S_0 v / G_s$ at which a transition from a planar to cellular interface was observed in the experiments. (b) Areal coverage of *c*-axis horizontal crystals in the top thin sections compared to the depth of a stably stratified surface layer, the base of which is taken to be the point where the measured temperature is above the temperature of maximum density. No top thin section was taken for the $S = 1.2$ ppt experiment, but we infer that no horizontal *c*-axis crystals were present based on inspection of the middle horizontal thin section and the vertical thin section. Uncertainties are derived from thermistor spacing and the measurement of θ.

study, the maximum density of the water will occur at a temperature of $3.55°C \leq T_{\rho\text{-max}} \leq 3.98°C$. At the surface where the water is colder than $T_{\rho\text{-max}}$, temperature and hence density will increase monotonically with depth. We therefore do not expect convection in this surface layer. Deeper water, however, will be warmer than $T_{\rho\text{-max}}$ (unless the whole tank was initially colder than $T_{\rho\text{-max}}$). We expect convection in this warmer region. Specifically, convection is presumed to occur at and below the shallowest thermistor with a temperature above $T_{\rho\text{-max}}$. The thickness of the quiescent surface layer is therefore the region above this. Thermistors are spaced 10 mm apart, giving a ± 5 mm uncertainty in the thickness.

For our small number of experiments with brackish water, we observe the expected trend of a decreasing proportion of horizontal *c*-axis crystals with increasing depth of the stably stratified layer (Figure 4b). Our freshwater experiment, however, does not fit this trend. In this experiment, only the thermistor immediately at the surface measured a temperature below $T_{\rho\text{-max}}$.

5. Conclusion

Coincident changes in ice–water interface morphology and crystal orientation below the initial ice cover were observed when the salinity of tank water was increased from 1.2 ppt to 2.0 ppt. We attribute this to constitutional supercooling becoming significant at the higher salinity. Given the controlled conditions for our experiments, it was assumed that seeding of the initial ice cover did not influence the initial crystal orientation. Instead, our experiments suggested that the prevalence of *c*-axes vertical crystals is coupled to thickness of a stably stratified layer of water at the surface.

References

Dumont, H. J. 1998. The Caspian Lake: history, biota, structure, and function. *Limnol. Oceanogr.*, 43(1), 44–52. doi:10.4319/lo.1998.43.1.0044

Gow, A. J. 1986. Orientation textures in ice sheets of quietly frozen lakes. *J. Cryst. Growth.,* 74(2), 247–258. doi:10.1016/0022-0248(86)90114-4

Gow, A. J. and Ueda, H. T. 1989. Structure and temperature dependence of the flexural properties of laboratory freshwater ice sheets. *Cold Reg. Sci. Tech.*, 16(3), 249–270. doi:10.1016/0165-232X(89)90026-8

Gow, A. J., Weeks, W. F., Kosloff, P and Carsey, S. 1992. Petrographic and salinity characteristics of brackish water ice in the Bay of Bothnia. CRREL Report 92-13.

Granskog, M. A., Uusikivi, J., Blanco Sequeiros, A. and Sonninen, E. 2006. Relation of ice growth rate to salt segregation during freezing of low-salinity sea water (Bothnian Bay, Baltic Sea). *Ann. Glaciol.*, 44(1), 134–138. doi:10.3189/172756406781811259

Knight, C. A., 1962. Studies of Arctic lake ice. *J. Glaciol*., 4(33), 319–335.

Langway, C. C. 1958. Ice fabrics and the universal stage. Technical Report, vol. 62, U.S. Snow Ice and Permafrost Research Establishment.

Müller-Stoffels, M., Langhorne, P. J., Petrich, C. and Kempema, E. W. 2009. Preferred crystal orientation in fresh water ice. *Cold Reg. Sci. Tech.* 56(1), 1–9. doi:10.1016/j.coldregions. 2008.11.003

Palosuo, E. 1961. Crystal structure of brackish and fresh-water ice. International Association of Science Hydrology Publication 54 (General Assembly of Helsinki 1960–Snow and Ice), 9–14.

Perey, F. G. J. and Pounder, E. R. 1958. Crystal orientation in ice sheets. *Can. J. Phys.*, 36(4), 494–502. doi:10.1139/p58-050

Ryves, D. B., Clarke, A. L., Appleby, P. G., Amsinck, S. L., Jeppesen, E., Landkildehus, F. and Anderson, N. J. Reconstructing the salinity and environment of the Limfjord and Vejlerne Nature Reserve, Denmark, using a diatom model for brackish lakes and fjords. *Can. J. Fish. Aquat. Sci.*, 61(10), 1988–2006. doi:10.1139/F04-127

Tiller, W. A., Jackson, K. A., Rutter, J. W. and Chalmers, B. 1953. The redistribution of solute atoms during the solidification of metals. *Acta Metall.,* 1, 428–437. doi:10.1016/0001-6160(53)90126-6

Weeks, W. F. and Ackley, S. F. 1986. The growth, structure, and properties of sea ice. In *The Geophysics of Sea Ice*, edited by N. Untersteiner, 9–164. Plenum Press. doi:10.1007/978-1-4899-5352-0_2

Weeks, W. F. and Lofgren, G. 1967. The effective solute distribution during the freezing of NaCl solutions. In *Physics of Snow and Ice: International Conference on Low Temperature Science, Proceedings, vol. 1*, edited by H. Oura, 579–597. Inst. Low Temp. Sci, Hokkaido.

Weeks, W.F. 2010. *On Sea Ice*. University of Alaska Press.

Wettlaufer, J. S. 1992. Directional solidification of salt water: deep and shallow cells. *Europhys. Lett*., 19(4), 337–342. doi:10.1209/0295-5075/19/4/015